Atmospheric vortex streets on a RADARSAT SAR image

Xiaofeng Li[1], Pablo Clemente-Colón[2], William G. Pichel[2] and Paris W. Vachon[3]

[1]Research and Data Systems Corporation, NOAA E/RA3, WWBG, Room 102
5200 Auth Road, Camp Springs, MD 20746-4304, U.S.A.
xiaofeng.li@noaa.gov

[2]NOAA/NESDIS, NOAA E/RA3, WWBG, Room 102
5200 Auth Road, Camp Springs, MD 20746-4304, U.S.A.

[3]Canada Centre for Remote Sensing
588 Booth St., Ottawa, Ontario K1A 0Y7, Canada

Abstract

We analyze the sea surface imprint of two atmospheric vortex streets (AVS's) observed on a RADARSAT, a Canadian earth observation satellite, Synthetic Aperture Radar (SAR) image of the Aleutian Islands in the western Gulf of Alaska acquired on May 5, 1999. The RADARSAT SAR instrument is operated in C-band with HH polarization. These AVS's are interpreted as the atmosphere analog of classic Von Kármán vortex streets. The SAR image, along with radiosonde data and surface weather charts, reveal that the AVS lengths are 196 km and 111 km for AVS-1 and AVS-2, respectively. There are five and two pairs of vortices within each AVS. The vortex shedding period is estimated to be between 35 and 48 minutes. The vortex shedding started approximately 4.6 and 2.6 hours prior to the SAR imaging time for AVS-1 and AVS-2, respectively. There are seven and three pairs of vortices within the respective AVS's. The vortex tangential velocity is estimated to be between 1.7 and 2.3 m/s and the energy dissipated during the vortex lifetime is estimated to be between 24.9 and 23.6 J/m^3.

1. Introduction

When air flows around an obstacle, such as a mountain or island, atmospheric vortex streets (AVS's) can develop on the lee side of the obstacle under favorable conditions. The AVS pattern consists of a double row of counter rotating vortex-pairs shedding alternately near each edge of the obstacle and resembles the classic Von Kármán vortex-street patterns observed in laboratory flow experiments and illustrated in Figure 1. Although atmospheric vortex shedding from large islands was suggested as early as the 1930's (Lattau, 1939), it was not until the early 1960's that researchers (e.g. Hubert and Krueger, 1962; Chopra and Hubert, 1964; 1965) observed the AVS pattern in the atmosphere in cloud images taken by the first generation of earth orbiting satellites. AVS's were not observed prior to the advent of satellites due to the AVS scale of 100 to 400 km; too small to be delineated by a synoptic observation network and too large to be observed by a single station (Chopra and Hubert, 1964; Etling, 1989).

The wind field associated with an AVS causes cloud structure to change around the obstacle allowing the AVS to be observed in satellite cloud images. Based on Von Kármán vortex theory, Chopra and Hubert (1964; 1965) analyzed TIROS-VI cloud images of the Madeira Island (32^{o}N, 17^{o}W) and were able to derive the characteristics of AVS's, including the ratio of vortex row to vortex spacing, the vortex shedding period, their life time, the displacement speed, and the drag coefficient. Milkins (1968) estimated the tangential velocity at the edge of the AVS and found that the dissipation rate of a 3-

hour old vortex is about two orders of magnitude greater than the background turbulence. Tsuchiya (1969) analyzed two successive TIROS cloud images in the wake of Cheju Island in the Northwest Pacific and concluded that the cloud pattern can be interpreted as an atmospheric analogue of the Von Kármán vortex street. In addition, he found that the AVS parameters extracted from the satellite images are in good agreement with theoretical calculations. Thomson *et al.* (1977) analyzed a NOAA satellite image and discussed the drag coefficient and vortex viscosity for a regular symmetrical wake and an irregular asymmetrical wake. Etling (1989; 1990) conducted laboratory experiments and found that mesoscale vortex shedding by a three dimensional obstacle is influenced by both flow stratification and rotation. He also suggested that geostationary satellite images with a temporal resolution of 30 minutes would be useful for validating the vortex shedding frequency estimated by theory.

The surface wind field associated with an AVS can also modify the sea surface roughness. A synthetic aperture radar (SAR) senses the ocean surface roughness through a Bragg scattering mechanism. Therefore, SAR can observe any atmospheric process that modulates near surface wind field. Examples include lee waves, gravity waves, boundary layer rolls, atmospheric fronts, and mesoscale phenomena such as polar mesoscale cyclones and hurricanes (see the most recent review by Mourad, 1999). In general, the brighter ocean regions can be interpreted as regions of higher wind speed. In this paper, we present and analyze one of the first examples (of which we are aware of) of AVS's observed on a RADARSAT SAR (Raney, et al. 1991) image. The scales of these AVS's are smaller than those of previous case studies.

2. Atmospheric vortex street patterns on a RADARSAT SAR image

The RADARSAT SAR image (Figure 2) considered in this study was extracted from a ScanSAR Wide B scene that was processed at the Alaska SAR Facility as a QuickLook product (i.e., to a spatial resolution of 200 m with a pixel spacing of 100 m). The image center is at roughly 52^{o}N, 172^{o}W and covers the western side of the Gulf of Alaska. The image was acquired at 17:25:41 UTC on May 5, 1999. The bright round features at the top of the image are the Islands of Four Mountains of the Aleutian Islands. The two AVS's were generated in the wake of Herbert Island (AVS-1) and Chuginadak Island (AVS-2), respectively. The dark pattern in the middle of the AVS represents the low backscatter from a smoother sea surface associated with lower wind speed in the island's lee shadow region. The bright spots on either side of the low wind speed pattern are the atmospheric vortices. The AVS pattern length is less than 200 km on the lee side of the islands. This length is smaller than that of the previous cases considered in the literature; the AVS length is usually about 400 to 500 km.

Figure 3 shows the topography of the Islands of Four Mountains. The island cross stream diameters for Herbert Island (d_1) and Chuginadak Island (d_2), as measured at the inversion layer level (see below), are about 7.6 km.

The virtual and dew point temperature data, measured at the nearest radiosonde station (Saint Paul Island, Alaska (57 ^{o}25'N, 170 ^{o} 33' W)) at 1200 Z on May 5, 1999, show a

strong, narrow inversion layer at a height of about 1200 m, with a mean air temperature increase of between 2^{o}C and 4^{o}C. Within the height range from 100 m to 1200 m, the wind vector is about 15.9 m/s from 290^{o} with respect to north. The radiosonde station is about 200 km north of the image center. These observations were taken about five hours prior to the SAR acquisition time. The atmospheric stratification parameters for the radiosonde station may differ from those existing within the imaged area due to location and time differences. However, it is reasonable to use this radiosonde data to represent the atmosphere conditions at the actual imaging time for the following reasons. First, there are at least seven pairs of vortices in AVS-1. This indicates that atmosphere stratification must have remained relatively stable over a long period of time to support the vortex shedding. Second, the NOAA National Centers for Environmental Prediction surface pressure analysis weather charts (not shown here) show that the radiosonde station location and the SAR image were dominated by the same atmospheric system at 1200Z and 1800Z. The weather system did not move appreciably between 1200Z and 1800Z. The Islands of Four Mountains and the radiosonde station fall between the same surface pressure contour lines.

3. Properties of atmospheric vortex streets

3.1 The ratio of vortex row to vortex spacing ($h/\bar{a}$)

The ratio $h/\bar{a}$ (see Figure 1) is a basic property of an AVS. Laboratory experiments show that a stable vortex formed on the lee side of an obstacle is characterized by $0.28 < h/\bar{a}$

<0.52 (Chopra and Hubert, 1964). $h/\bar{a}$ for the Madeira Island (Chopra and Hubert, 1965) and Cheju Islands (Tsuchiya, 1969) case studies were 0.43 and 0.33, respectively. Five AVS patterns observed near the Aleutian Islands by Thomson *et al.* (1977) had $h/\bar{a}$ between 0.30 and 0.60.

In our case, the dimensions of the two AVS patterns are measured directly from the RADARSAT SAR image and are given in Table 1. The $h/\bar{a}$ ratio is 0.41 for AVS-1 and 0.44 for AVS-2. One can see that the $h/\bar{a}$ varies, even over the same AVS. This is because the vortex shedding depends on the size and shape of the obstacle as well as the flow characteristics. In this case, the AVS created by different obstacles from more than one island is thought to be the main reason for the variation of $h/\bar{a}$. We use the ideal wind field to estimate the basic properties of the AVS, so the average values of $h/\bar{a}$ will be used in the following analysis.

From Table 1, one can see that the average spacing is 24.6 km for AVS-1 and 34.8 km for AVS-2. These vortex spacing are much smaller than those observed by Thomson *et al.* (1977) in the Aleutian Islands (i.e., 50 to 85 km). The AVS length is measured to be 196 km for AVS-1 and 111 km for AVS-2.

3.2 Vortex shedding rate (f) and propagation velocity (U_e)

The AVS vortex shedding rate f is defined by Chopra and Hubert (1964):

$$f = \frac{Ue}{\bar{a}} = \frac{U_o}{\bar{a}}\left(\frac{U_e}{U_o}\right) \quad (1)$$

where f is the vortex shedding rate or frequency. U_e is the vortex propagation velocity, and U_o is the undisturbed wind velocity. The relationship between U_e and U_o is given by Chopra and Hubert (1965):

$$U_o - U_e = (k / 2\bar{a})\tanh(\pi h / \bar{a}) \quad (2)$$

where k is the circulation strength:

$$k = \int_0^R \zeta dA = 2\pi R V_\theta \quad (3)$$

where R is the vortex radius, ζ is the vortex vorticity, and V_θ is the tangential vortex velocity at the vortex outer edge.

From Eqs. 1 and 2 we derive:

$$fk = 2U_e(U_o - U_e)\coth(\pi h / \bar{a}) \quad (4)$$

In Eq. 4, $h/\bar{a}$ can be measured from SAR image directly, and U_o can be obtained from radiosonde measurements. However, U_e and k are unknown. U_e can be measured from consecutive remote sensing images, if available, that show the evolution of the same AVS. However, in our case, only one SAR image is available. Another way to estimate

U_e is by using the drag definition and Eq. 4. Chopra and Hubert (1965) derived the drag D as:

$$D = \rho hfk = 2\rho hU_e(U_O - U_e)\coth(\pi h/\bar{a}) \tag{5}$$

where, ρ is the density of the fluid. The drag can also be derived from another theory (Birkhoff and Zarantonello, 1957) as:

$$D = \frac{\rho k^2}{2\pi\bar{a}} + \frac{\rho kh}{\bar{a}}(2U_e - U_O) \tag{6}$$

The above equations are equal, so that Eqs. 5 and 6 yield (Tsuchiya, 1969):

$$(2B - A)\left(\frac{U_e}{U_O}\right)^2 + (2A - 3B)\left(\frac{U_e}{U_O}\right) + \left(-A + B + \frac{B}{4A}\right) = 0 \tag{7}$$

where A=coth($\pi h/\bar{a}$) and B= $\pi h/\bar{a}$. For the special case A=B (Chopra and Hubert, 1964; 1965; Tsuchiya, 1969), we have $h/\bar{a} \approx 0.39$. Therefore, for the $h/\bar{a}$ close to 0.39, Eq. 7 becomes:

$$4\pi(h/\bar{a})(U_e/U_O)(1 - U_e/U_O) = 1 \tag{8}$$

There are up to two real positive solutions for U_e/U_o from Eq. 8. If two real solutions exist, only the larger one will apply. In our case, $h/\bar{a}$ is 0.41 for AVS-1 and 0.44 for AVS-

2. Therefore, U_e/U_o for AVS-1 and AVS-2 are 0.74, and 0.76, respectively. The vortex shedding rate f can then be calculated from U_e and the $\bar{a}$ as:

$$f = \frac{U_e}{\bar{a}} \tag{9}$$

Knowing the length (L) of the AVS, one can then calculate the vortex life time (τ) as:

$$L = U_e \tau \tag{10}$$

In our case, U_o is about 15.9 m/s, L_1=196 km, and L_2=111 km. Using Eqs. 8 and 9, we estimate that τ_1= 4.6 hr, τ_2= 2.6 hr, shedding frequency f_1=4.8×10^{-4} s^{-1}, f_2=3.5×10^{-4} s^{-1}, and shedding period T_1= 35 minutes, T_2= 48 minutes.

3.3 Reynolds, Strouhal, and kinematic vortex viscosity numbers

Etling (1990) showed that a stable vortex on the lee side of an obstacle can exist when the Reynolds Number (*Re*) is larger than a critical value and the Froude number is smaller than 0.4. Tsuchiya (1969) showed that a vortex can exist when 60 < *Re* < 5000. The Reynolds Number is given as:

$$Re = \frac{U_O d}{\upsilon} \tag{11}$$

where d is the obstacle diameter, and ν is the kinematic viscosity. Since ν of Eq. 11 is unknown in most cases, it is impossible to estimate *Re* directly. Two other parameters, the Strouhal number (S) and the Lin Number (β), are introduced (Lin, 1959):

$$S = \frac{fd}{U_o} \tag{12}$$

$$\beta = \frac{S}{\mathrm{Re}} = \frac{f\upsilon}{U_o^2} \tag{13}$$

From Eq. 13, one can see that β does not depend on the shape and height of the obstacle. Therefore, β is an inherent property of AVS.

The range of β values given by Lin (1959) from laboratory experiments is:

$$10^{-3} < \beta < 2.5\times10^{-3} \tag{14}$$

If the vortex shedding rate f and wind speed U_o are known, one can use Eq. 13 to estimate the range of ν based on the range of β, and Eq. 11 to estimate the range of *Re*. Chopra and Hubert (1964, 1965) and Tsuchiya (1969) used this method in their case studies.

Using the vortex shedding rate f from Eq. 9 and the observed wind velocity U_o at the height of inversion layer, we estimate that $91 < Re < 229$ for AVS-1 and $66 < Re < 166$ for AVS-2. We estimated the kinematic viscosity (ν) to be $528<\nu<1321$ for AVS-1 and $728<\nu<1820$ for AVS-2. These numbers are comparable to the $O(10^3)$ kinematic

viscosity observed by Thomson *et al.* (1977) associated with vortex shedding events in the Aleutian Islands.

The Froude number (F) is defined as:

$$F = \frac{U}{\sqrt{gd}} \tag{15}$$

where d is the depth of the stream taken as the depth of the inversion layer (1200 m obtained from radiosonde measurements). Therefore, F = 0.15. This result is in the range of Froude numbers that could support vortex shedding (F < 0.4), as found by Etling (1990).

3.4 Vorticity and energy dissipation

The vortivity for an atmospheric vortex is mainly in the vertical direction. After neglecting the horizontal vorticity, Wilkins (1968) derived the rate of viscous dissipation of vortex energy within a cylindrical volume of radius R as:

$$\varepsilon = 2\pi\rho\upsilon \int_0^R \zeta^2 r dr \tag{16}$$

where R is the vortex radius, ε is the rate of viscous dissipation of vortex energy, ν is the kinematic viscosity, and ζ is the vortex vorticity. The vortex is assumed to be symmetrical, and ζ has the form:

$$\zeta = \frac{k}{4\pi\upsilon t} e^{(-r^2/4\upsilon t)} \tag{17}$$

Substituting Eq. 17 into Eqs. 3 and 16, we get:

$$V_\theta = (k/2\pi R)[1 - e^{(-R^2/4\upsilon t)}] \tag{18}$$

$$\varepsilon = (k^2/8\pi^2 R^2 t)[1 - e^{(-R^2/2\upsilon t)}] \tag{19}$$

where, k and ν are calculated from Eqs. 4 and 13. In this case, the vortex diameter is measured to be about 4 km for both AVS-1 and AVS-2. Therefore, we estimate that V_θ is 2.3 m/s for AVS-1 and 1.7 m/s for AVS-2. These values are about 50% smaller than those estimated by Wilkins (1968), presumably because the sizes and strength of the vortices in this case are much smaller.

The total energy dissipated by a vortex during its lifetime is given by (Wilkins,1968):

$$\frac{1}{\rho_o}\int_{t_o}^{\tau} \varepsilon dt = \frac{1}{\rho_o}(k^2/16\pi^2 \nu t_o)[1 + \sum_{n=1}^{\infty} \frac{(-R/2\upsilon t_o)^n}{(n+1)\cdot(n+1)!}] \tag{20}$$

In Eq. 20, ρ_o is the air density (≈1 kg·m^{-3}), t_o is the starting time and should be small compared to τ (Wilkins, 1968), and hence we choose t_o an order of

magnitude smaller than τ. Using the parameters for this case, we obtain the total energy for the oldest AVS-1 and AVS-2 vortices as 24.9 J/m^3 and 23.6 J/m^3, respectively. For practical purpose, only the first ten terms of Eq. 19 are calculated; the higher order terms are sufficiently small to be neglected. These numbers are of the same order but smaller than the case study of Wilkins (1968). The energy dissipation in his study was 840 ergs/cm^3 = 84 J/m^3. Again, the size and velocity of the vortex in his study were much larger.

4 Conclusions

Two atmosphere vortex streets were observed on a RADARSAT ScanSAR Wide B SAR image of the Aleutian Islands chain. They are interpreted as the atmosphere analog of classic Von Kármán vortex streets. The length of the two AVS's was measured to be about 196 and 111 km, respectively. The ratio of the width of the Von Kármán vortex street (h) and the vortex spacing ($\bar{a}$) was between 0.41 and 0.44. On the basis of this SAR image and a nearby radiosonde observations, the vortex shedding period was estimated to be 35 and 48 minutes for AVS-1 and AVS-2, respectively. The tangential velocity at the outer edge of the vortex was estimated to be about 2.3 m/s for AVS-1 and 1.7 m/s for AVS-2. The vortex lifetime at the SAR acquisition time was about three hours and the total energy dissipation was 24.9 J/m^3 for AVS-1 and 23.6 J/m^3 for AVS-2.

From this analysis, we see that if AVS patterns are observed by consecutive remote sensing images, the propagation velocity (U_e) and the length (L) may be measured from the images, thus allowing direct calculation of the vortex shedding rate (f) and lifetime (τ).

In order to observe the AVS, visible and infrared sensors require a high atmosphere moisture content so that clouds associated with the AVS wind pattern can be imaged. The SAR does not have this constraint since it images the sea surface imprint of the AVS. SAR coupled with visible and infrared sensors could provide the top and bottom patterns of the AVS. As the number of SAR sensors increases over the coming years, it is likely that simultaneous imaging (SAR, visible, and infrared) of an AVS will become available for more detailed AVS studies.

ACKNOWLEDGMENTS

This research was funded by the NOAA/NESDIS Ocean Remote Sensing Program. RADARSAT SAR data was obtained under NASA RADARSAT ADRO Project #396 and processed by the Alaska SAR facility. Radiosonde data were downloaded from the University of Wyoming Atmosphere Science Department web site at http://www-das.uwyo.edu/upperair. James Partain provided the NOAA/NCEP surface weather charts.

REFERENCES

Birkhoff, G and E. H. Zarantonello, *Jets, wakes and cavities*, New York, Academic Press, 353-354,1957.

Chopra, K. P. and L. F. Hubert, Kármán vortex streets in earth's atmosphere, *Nature, 203*, 1341-1343, 1964.

Chopra, K. P. and L. F. Hubert, Mesoscale eddies in wake of islands, *J. Atmos. Sci., 22*, 652-657, 1965.

Etling, D., On atmospheric vortex streets in the wake of large islands, *Meteorol. Atmos. Phys.*, 41, 157-164, 1989.

Etling, D., Mesoscale vortex shedding from large islands: A comparison with laboratory experiment of rotating stratified flows, *Meteorol. Atmos. Phys.*, 43, 145-151, 1990.

Hubert, L. F. ands A. F. Krueger, Satellite pictures of mesoscale eddies, *Mon. Wea. Rev., 90*, 457-463, 1962.

Lin, C. C., On periodically oscillating wakes in the Øseen approximation, *Studies in fluid mechanics*, New York, Academic Press, 170-176, 1959.

Milkins, E. M., Energy dissipated by atmospheric eddies in the wake of islands, *J. Geophys. Res., 73*, 1877-1881, 1968.

Mourad, P.D., 1999. Footprints of Atmospheric Phenomena in Synthetic Aperture Radar Images of the Ocean Surface- a review. Chapter 11 in "*Air-sea fluxes -physics, chemistry, and dynamics"*, edited by G. Geernaert, *Kluwer Academic Publishers*, Dordrecht, Holland, 640pp.

Raney, R.K., A. P. Luscombe, E. J. Langham, and S. Ahmed, RADARSAT, Proc. IEEE, 79, 6: 839-849, 1991.

Thomson, R. E., J. F. R. Gower and N. W. Bowker, Vortex streets in the wake of the Aleutian Islands, *Mon. Wea. Rev., 105*, 873-884, 1977.

Tsuchiya, K., The clouds with the shape of Kármán vortex street in the wake of Cheju Island, Korea, *J. Meteo. Soc. Japan, 47*, 457-464, 1969.

Turner, J. and D. E. Warren, A multi-spectral satellite image of a vortex street in the lee of Jan Mayen, *Weather, 43*, 363-369, 1988.

Table 1. Properties of the two atmosphere vortex streets (AVS's) observed on a RADARSAT SAR image: h is the lateral spacing between the two vortex rows; and ā is the longitudinal spacing between two vortices in the same row.

AVS-1	Seven vortex pairs exist on the lee side of Herbert Island (the first 5 pairs of vortices are measured)									
	Western row					Eastern row				
Vortex pair	1	2	3	4	5	1	2	3	4	5
$\bar{a}_1$ (km):	24.3	23.2	22.0	27.6	22.5	24.8	25.2	24.4	20.3	32.1
h_1 (km):	8.4	10.0	10.4	10.0	11.2	8.4	10.0	10.4	10.0	11.2
$h_1/\bar{a}_1$	0.35	0.43	0.47	0.36	0.50	0.34	0.40	0.43	0.49	0.32
Average	$\bar{a}_1$= 23.9, h_1=10.0 , $h_1/\bar{a}_1$=0.42					$\bar{a}_1$= 25.3, h_1=10.0 , $h_1/\bar{a}_1$=0.40				

AVS-2:	Three vortex pairs exist on the lee side of Chuginadak Island									
	Western row					Eastern row				
Vortex pair	1	2				1	2			
$\bar{a}_2$ (km):	34.4	37.5				32.8	34.3			
h_2 (km):	14.4	16.6				14.4	16.6			
$h_2/\bar{a}_2$	0.42	0.44				0.44	0.48			
Average	$\bar{a}_2$=36.0 , h_2=15.6 , $h_2/\bar{a}_2$=0.43					$\bar{a}_2$=33.6 , h_2=15.6 , $h_2/\bar{a}_2$=0.46				

Figure captions:

Figure 1. Schematic plot of a Kármán vortex street generated by wind passing a cylindrical obstacle of diameter *D*. $\bar{a}$ is the vortex spacing, and *h* is the width of the Kármán vortex street.

Figure 2. A RADARSAT ScanSAR wide B SAR subimage containing the sea surface imprint of two atmospheric vortex streets. The image center is located at roughly N52^{o} and W172^{o}, and covers the western side of the Gulf of Alaska. The image was acquired at 17:25:41 UTC on May 5, 1999. (© Canadian Space Agency, 1999)

Figure 3. The side (a) and top (b) view of the topography of the Islands of Four Mountains, a part of the Aleutian Islands chain. The topography map is generated from the Digital Terrain Elevation Data (DTED®) in the National Imagery and Mapping Agency (NIMA) standard digital dataset. The atmospheric vortex streets in Figure 2 were observed on the lee side of Herbert Island and Chuginadak Island.

Figure 1.

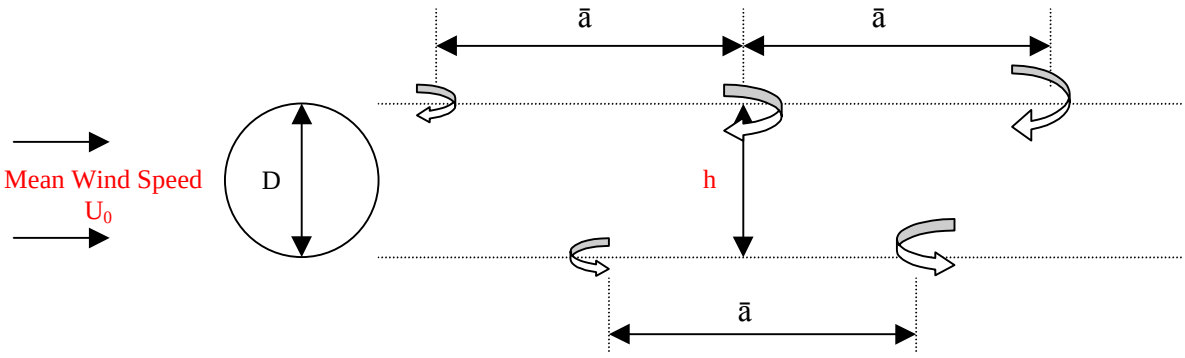

Figure 2.

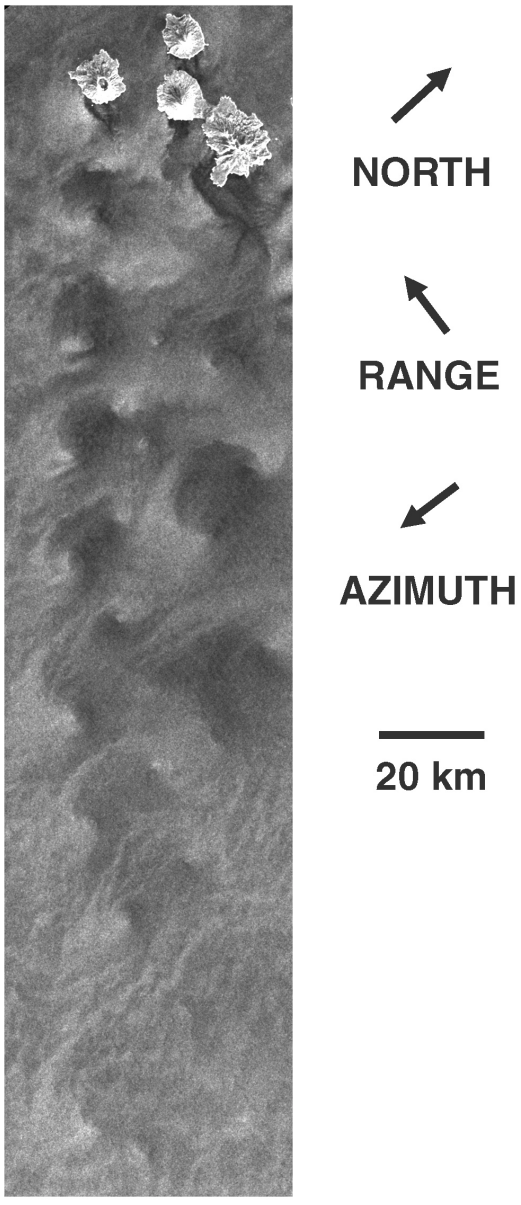

Figure 3.

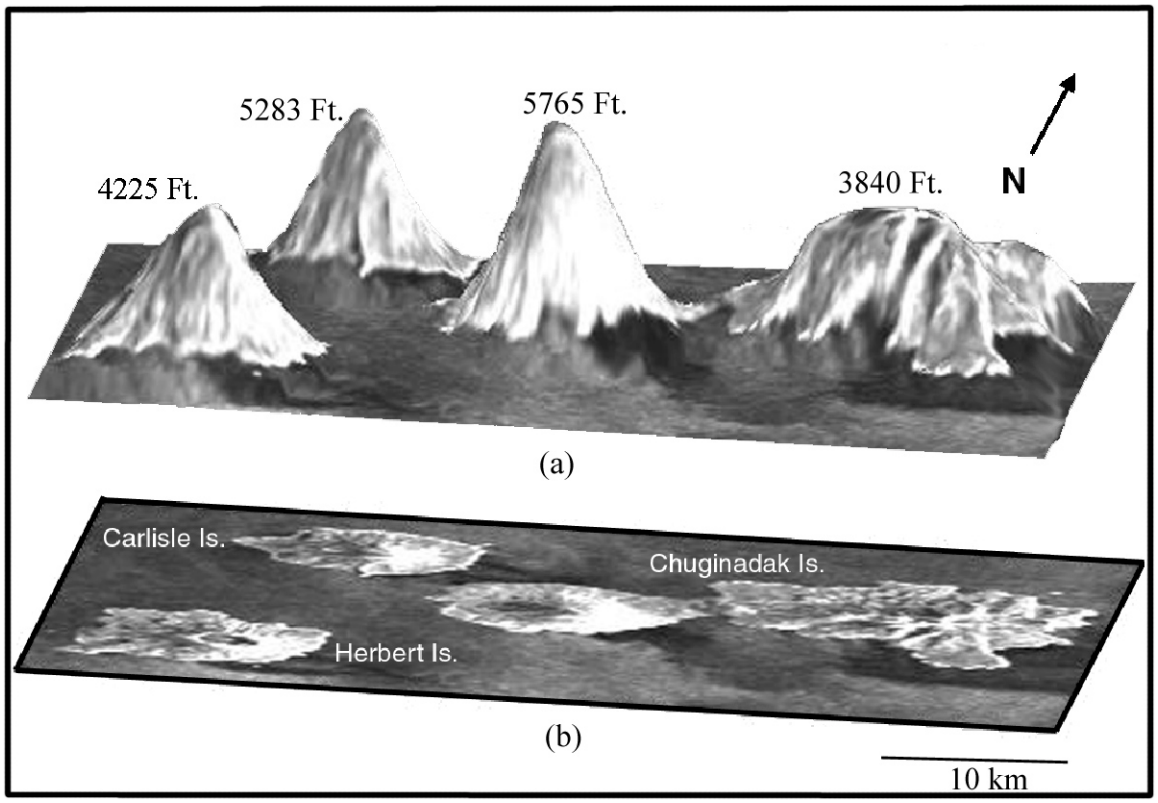
5283 Ft.
5765 Ft.
4225 Ft.
3840 Ft.
N
(a)
Carlisle Is.
Chuginadak Is.
Herbert Is.
(b)
10 km